ACS central science

http://pubs.acs.org/journal/acscii

Research Article

High-Throughput Evaluation of Emission and Structure in Reduced-Dimensional Perovskites

Husna Anwar,[▽] Andrew Johnston,[▽] Suhas Mahesh, Kamalpreet Singh, Zhibo Wang, Douglas A. Kuntz, Isaac Tamblyn, Oleksandr Voznyy, Gilbert G. Privé, and Edward H. Sargent*

Cite This: *ACS Cent. Sci.* 2022, 8, 571−580

Read Online

ACCESS | Metrics & More | Article Recommendations | Supporting Information

ABSTRACT: High-throughput experimentation (HTE) seeks to accelerate the exploration of materials space by uniting robotics, combinatorial methods, and parallel processing. HTE is particularly relevant to metal halide perovskites (MHPs), a diverse class of optoelectronic materials with a large chemical space. Here we develop an HTE workflow to synthesize and characterize light-emitting MHP single crystals, allowing us to generate the first reported data set of experimentally derived photoluminescence spectra for low-dimensional MHPs. We leverage the accelerated workflow to optimize the synthesis and emission of a new MHP, methoxy-phenethylammonium lead iodide ($(4\text{-MeO-PEAI})_2\text{-PbI}_2$). We then synthesize 16 000 MHP single crystals and measure their photoluminescence to study the effects of synthesis parameters and compositional engineering on the emission intensity of 54 distinct MHPs: we achieve an acceleration factor of more than 100 times over previously reported HTE MHP synthesis and characterization methods. Using insights derived from this analysis, we screen an existing database for new, potentially emissive MHPs. On the basis of the Tanimoto similarity of the bright available emitters, we present our top candidates for future exploration. As a proof of concept, we use one of these (3,4-difluorophenylmethanamine) to synthesize an MHP which we find has a photoluminescence quantum yield of 10%.

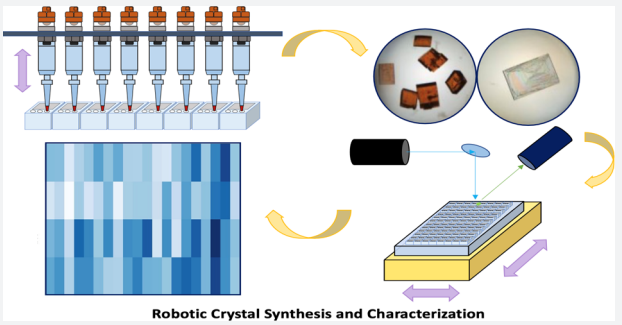

INTRODUCTION

Metal halide perovskites (MHPs) have the general formula ABX_3, where A is a small cation such as methylammonium (MA) or Cs^+, B is a larger cation such as Pb^{2+}, and X is a halide. Ideal MHPs have balanced electron and hole mobilities greater than 10 $cm^2\ V^{-1}\ s^{-1}$, free-carrier densities exceeding $10^{17}\ cm^{-3}$, and gain coefficients greater than $10^4\ cm^{-1}$.[1] MHPs are spectrally tunable through compositional or structural engineering; this allows for fine control of the photoluminescence (PL) spectra.[2−6] Taken together, these properties position MHPs for use in light emission applications such as energy efficient lighting, lasing, and displays.

In 1986, the Maruyama group introduced a new layered perovskite that combined organic and inorganic components to form a layered two-dimensional (2D) structure held together by van der Waals and intramolecular forces.[7] Here, the A site cation is replaced by a large organic aromatic or aliphatic ammonium cation.[8−13] In these reduced-dimensional perovskites, the large organic cation acts as a wide-band-gap spacer between the layers of the inorganic lead halide octahedra: the resulting structure can act as a quantum well. As these MHPs can easily be synthesized in sheets with spatially confined domains, they allow for greater tunability.[14,15] Quantum confinement, in part, leads to an increase in the optical band gap by ∼1 eV in 2D MHPs as well as inceased exciton binding energy.[16,17] Exciton binding energies in reduced-dimensional MHPs have been shown to exceed 400 meV, more than an order of magnitude higher than that of 3D MHPs (∼10 meV).[18−20] This enables efficient, narrow band emission, and as a result, 2D MHPs have found success as the active layer in light emitting diodes (LEDs).[21−25]

Red and green MHPs have demonstrated high photoluminescence quantum yields (PLQYs) of 90 and 70% respectively, narrow full width at half-maximum (fwhm) peaks of ∼20 nm, and LED quantum efficiencies of over 20%.[26−28] However, blue MHP LEDs require further engineering to achieve color stability.

Traditionally, blue emission in MHPs has been attained by using a mixture of Cl and Br in the X site.[29] Cl and Br based MHPs are difficult to fabricate using traditional synthesis techniques due to their poor solubility in popular solvents such as DMF and their sensitivity to synthesis conditions.[30] As a result, researchers have increasingly levered quantum confine-

Received: January 15, 2022
Published: May 6, 2022

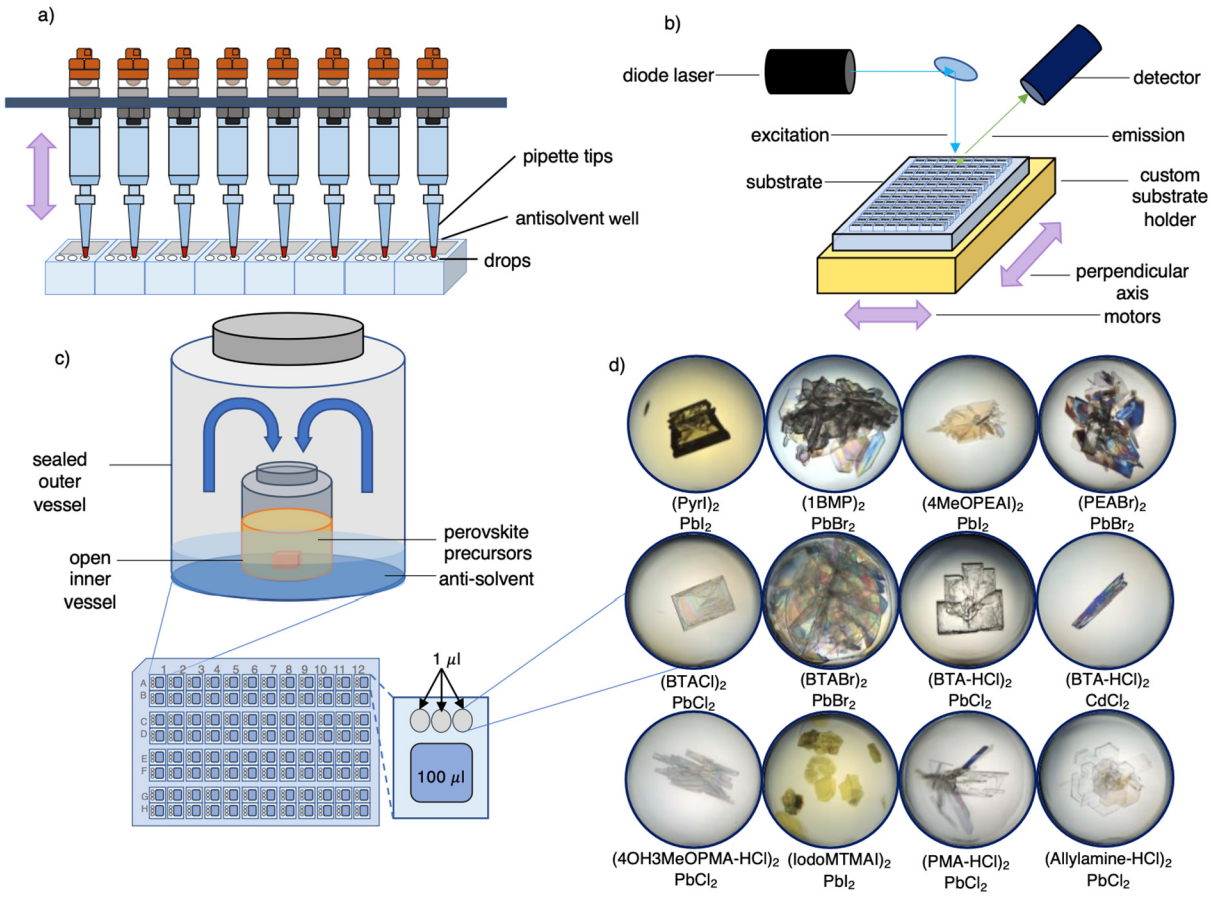

Figure 1. Overview of high-throughput experimentation and the acceleration achieved. (a) Schematic of the NT8 robot autopipetting system for high-throughput experimentation that achieves a 96 times acceleration over traditional VAAC synthesis. (b) Schematic of the automated photoluminescence measurement setup for high-throughput characterization that achieves a 140 times acceleration over traditional characterization methods. (c) (top) Schematic of a traditional vapor assisted antisolvent crystallization (VAAC) synthesis vessel compared to (bottom) the 96-well Intelliplate used for high-throughput synthesis. (d) Examples of the resulting MHP single crystals in the drops (full chemical names of ligands are in Table S1).

ment in nanoplatelets and nanocrystals to simultaneously achieve blue emission while avoiding synthetic and other issues, such as ion migration that degrades the color purity of blue emitters.[31] While the chemical space of reduced-dimensional MHPs is much larger than that of 3D perovskites, as the size of the organic ligands need not adhere to as strict a tolerance criterium, synthetic challenges have deterred researchers from exploring the available space.[32−34] These challenges impede the exploration and optimization of bright blue emitters and indicate that the discovery of blue MHPs can benefit from accelerated approaches.[35−37]

High-throughput experimentation (HTE) refers to the set of techniques that accelerate the rate at which experiments can be conducted. Its use in materials science is most mature in virology and protein synthesis, in which the experiments are conducted in an aqueous environment.

Combinatorial vapor deposition processes have been used to grow multiple thin films for the rapid screening of new material compositions; however, solution processable MHPs pose new challenges due to their reliance on volatile solvents that have low boiling points.[22] HTE has been employed in the exploration of MHPs, but until now it has been limited to several experiments on a single MHP or to the exploration of a few compositions with minimal processing conditions.[38−45]

MHP compositional exploration has focused primarily on polycrystalline thin films. The analysis of these films is obfuscated by the grain size and grain boundaries that arise during fabrication. Thus, the use of single crystals rather than thin films is preferable when studying fundamental properties of the MHPs. MHP single crystals can be grown easily with the use of a vapor assisted antisolvent crystallization (VAAC) process in which the MHP precursor solutions are left to crystallize while exposed in an antisolvent environment.[46−50] Recent studies have shown that the VAAC technique increases compositional homogeneity and reduces ion migration, making it ideal for synthesizing blue MHPs.[44] The slow antisolvent diffusion process can produce large, high-quality crystals that have not been demonstrated with the use of other methods.[5]

We thus took the view that developing a HTE workflow for the discovery of low-dimensional blue emitting MHP single crystals simultaneously addresses important challenges in the field. With this workflow we optimize the synthesis and emission of a 2D perovskite to demonstrate the validity of the process, complete 16 128 experiments on more than 50 MHPs, and use the insights to predict and synthesize a new blue perovskite, 3,4-difluorophenylmethanamine lead bromide, with 10% PLQY.

https://doi.org/10.1021/acscentsci.2c00041
ACS Cent. Sci. 2022, 8, 571−580

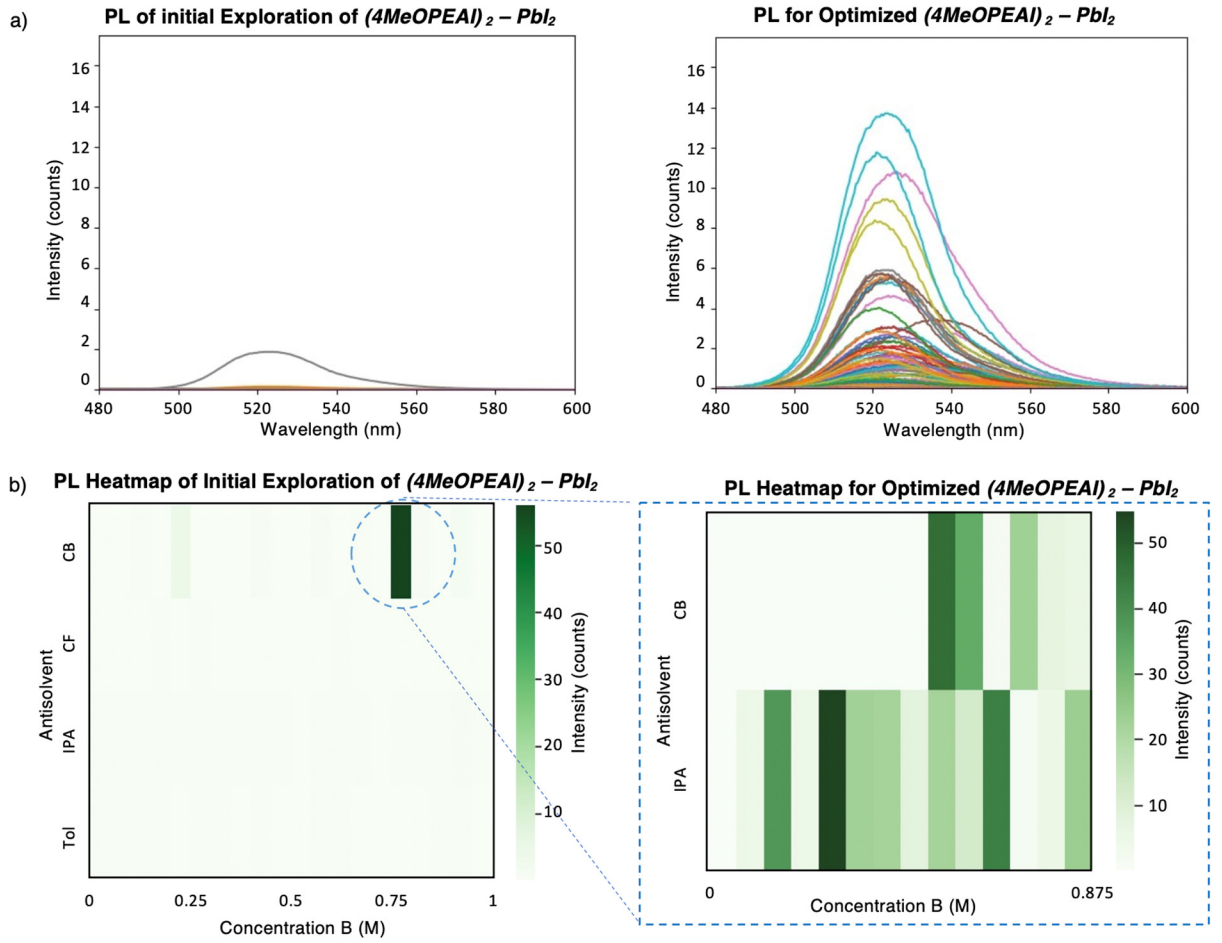

Figure 2. Validation of the HTE flow through the optimization of (4-MeO-PEAI)$_2$-PbI$_2$. (a) (4-MeO-PEAI)$_2$-PbI$_2$synthesis optimization: (left) plot showing the PL from the single crystal with a measurable PL after an exploration of a wide spread of concentrations and antisolvent conditions; (right) plot showing the PL curves for multiple (4-MeO-PEAI)$_2$-PbI$_2$ crystals grown using a narrower spread of optimized experimental parameters yielding a 7.5 times higher I_{max} for this previously unexplored material. (b) Heat map visualization: (left) initially, three drops yielded crystals; (right) narrowing the synthesis conditions that produced the brightest crystal yielded a 180 times increase in likelihood of crystals with emission (brightest crystals for each antisolvent, solvent, and precursor concentration combination are shown).

RESULTS AND DISCUSSION

High-Throughput-Experimentation Method. We previously repurposed an NT8 protein drop-setting robot (Figure 1a) to synthesize single crystal MHPs in high throughput.[51,52] In this proof-of-concept work, the robot was used to study a bright blue perovskite and the resulting images were used to train a convolutional neural network (CNN) to recognize the presence of a crystal. This exploration was limited to two materials, predicted just one new material, and did not characterize the emission of the crystals produced in high throughput. The methodology presented herein enables the exploration of a significantly larger number of perovskites and leads to the prediction of 18 new materials.

We developed a high-throughput-characterization (HTC) setup (Figure 1b) and expanded our chemical space to explore a variety of A site cations and X site halides. We used this to identify previously unexplored A-site ligands for bright emitters. The HTC is used to screen an Intelliplate protein growth plate, comprised of 288 synthesis drops clustered in groups of three next to an antisolvent well (Figure 1c). This autonomous characterization method can screen a full tray of 288 crystal drops in under 5 min. A full-time experimenter (FTE) might efficiently characterize a single crystal in 15 min: 288 crystals would take an FTE 72 h. Our flow also includes imaging the crystals as they form: Figure 1d shows the variety of crystals grown.

We validated our HTE flow by studying the perovskite (4-MeO-PEAI)$_2$-PbI$_2$ (Figure 2). We found that 576 experiments (two plates) were needed to optimize both the crystal growth parameters and maximum emission intensity (I_{max}): we were able to perform these experiments in <6 h of lab time. During the initial screening, only three of the 288 experiments produced crystals: two with chlorobenzene (CB) and one with isopropanol (IPA). Of these crystals, only one produced a measurable PL (Figure 2a). We fine-tuned the synthetic parameters by narrowing the range of precursor concentrations around this crystal and used only CB and IPA for our antisolvents. The resulting tray showed a 180 times greater success rate for crystals with emission and resulted in 7.5 times brighter PL than the initial screening (Figure 2b). We estimate that 576 experiments would take an FTE 1700 h in the lab (extrapolated from an average time of 3 h/experiment). A recently reported HTE process utilizing a robot-based arrayed synthesis technique would take over 9 h to synthesize 576 samples prior to characterization.[40]

Acceleration and Optimization of New MHP Composition. After validating our HTE workflow by optimizing (4-

https://doi.org/10.1021/acscentsci.2c00041
ACS Cent. Sci. 2022, 8, 571−580

MeO-PEAI)$_2$-PbI$_2$, we chose additional MHP precursors to study. Kanatzidis and co-workers[34] suggested the following heuristics for determining the suitability of an organic spacer for 2D MHPs: net positive charge, degree of substitution of the amine, hydrogen bonding capacity, stereochemical configuration, and space-filling ability. We used these metrics to select a large array of MHPs to study using our HTE. Our chosen ligands included organic ammonium cations with long-chain aliphatic groups as well as ligands with phenyl groups. We synthesized over 54 bromide, iodide, and chloride MHPs over 16 128 experiments with varied precursor concentrations and volumes, solvent combinations, and antisolvent choices.

We explored four to five materials per day (an average of 20 per week). Kirman et al. calculated that a single full-time experimenter (FTE) would need to conduct 560 experiments to explore the synthetic space for a single material,[51] estimating that the average researcher would try 20 precursor concentrations, at least four antisolvents, and seven combinations across three solvents. Of course, an FTE explores several materials simultaneously, but here the characterization process becomes the bottleneck: preparing samples and measuring their PL properties serially is time-consuming. We were able to measure between 1100 and 2300 crystal emission spectra daily (across four to eight materials). Our acceleration over Kirman et al. and a previously reported HTE method for MHP discovery is summarized below (Table 1).

Table 1. Summary of Previously Reported HTE Synthesis and Characterization Methods versus the HTE Method Reported in This Work

	previous HTE method[45]	Kirman et al.[51]	this work	our acceleration over previous HTE method
unique compositions/month	48	1	54	1.125×
A-site ligands/month	15	1	54	3.6×
samples prepared/month	144	1728	16000	112×
acceleration over FTE	35×	13×[a]	120×[a]	–

[a]Times estimate based on average in our group.

Insights and Discussion from Data Set. The data set generated by our HTE workflow also includes over 100 000 crystal images. The shape and emission of the crystals coincide with the cation dependence observed by Gong et al.: layered, flakelike crystals demonstrated narrow, sharp emission, while spiky needlelike crystals produced poor, broadband emission.[53] This effect was also observed in the upscaled macrocrystals for the materials (Figure S4). We compiled the emission spectra and experimental parameters and analyzed relative trends. We visualized the data generated from our workflow by normalizing and analyzing emission intensities across all the materials explored and extracted important indicators of color stability such as the full width at half-maximum (fwhm) (Figure 3a). We also explored the dependency of crystallization and emission on precursor concentration, solvent choice, and antisolvent choice. The heat map in Figure 3b shows the spread of emission intensity for (PEABr)$_2$-PbBr$_2$ with increasing precursor concentration plotted against antisolvent choice.

With the exception of PEABr, crystallization of the brightest blue emitters often occurred between 0.25 and 0.45 M. There was no linear trend apparent in increasing concentration and crystallization. Instead, we observed that crystallization occurs at optimal combinations of a certain solvent ratio, precursor concentration, antisolvent choice, and even precursor volume. We diluted the precursors with different ratios of *N*,*N*-dimethylformamide (DMF) and dimethyl sulfoxide (DMSO) to study the effect of this solvent system on crystallization kinetics. The addition of DMSO improved precursor solubility for brominated compounds and increased the crystal size and emissivity of the single crystals formed. This enhancement is due in part to the formation of the DMSO−PbBr$_2$ complex which slows crystallization and produces crystals of better quality.[54] In general, precursors dissolved in a 50−50 ratio of DMF and DMSO produced the strongest PL.

Given the skewed spread of I_{max}, we identified the five brightest crystals for each material and studied the synthetic parameters that produced them. The two aromatic antisolvents, CB and toluene (bp 132 and 111 °C, respectively), produced the majority of our brightest crystals, while chloroform (CF) and IPA (bp 61 and 82 °C, respectively) produced smaller and thinner crystals with relatively weaker emission. We found that CB and toluene produced 33 and 30% of the brightest crystals; toluene also produced 30% of the narrowest emitters. We investigated this effect further by studying the images gathered over the 7 days of crystallization, during which we imaged each crystal multiple times. We found that the boiling point (bp) of the antisolvent used influences the speed of crystal growth and, hence, the resulting size and emission of the crystals. Figure 3d shows the crystallization of (PEAI)$_2$-PbI$_2$ at day 2 (top) and day 5 (bottom). CF crystals form quickly but remain small, while toluene takes the longest to induce crystallization but produces the largest crystals and narrowest emission. We attribute this to the relative polarity of the antisolvents. Even though toluene has a bp comparable to that of CB, it is also less polar; a less polar antisolvent (that is still miscible with the solvent) is less likely to dissolve the perovskite precursor materials and produces larger crystals of better quality.

Additionally, we found that a 400 μL precusor volume produced smaller crystals (Figure 3e, left) when compared to a volume of 800 μL for the same precursor concentration and antisolvent. We also observed that a larger number of crystals were produced (Figure 3e, right). We posit that the increase in the number of crystals is because a smaller volume of solvent evaporates faster and the resulting saturated solution holds a greater number of PbX$_2$ nucleation sites. This is more apparent in the perovskites with lead halides that are less soluble in DMF and DMSO (bromide and chlorides).[55] Heterogenous nucleation, the mechanism wherein the crystallization process is initiated by an external nucleation site, can dictate the formation kinetics of the crystals.[56]

Hence, we show that controlling the volume and spread of the precursor solution can influence the presence of heterogeneous nucleation sites and, thus, the morphology of polycrystalline perovskite films.

We also observed a slight shift in the emission peaks for methoxy- and hydroxy-functionalized PEA derivatives, both for PEABr and for PEAI (Figure S4). We studied the blue shift in the peak position for 4-MeO-PEABr with density functional theory (DFT) calculations (Figures S1 and S2). The methoxy compound in the *para* position acts as an electron-donating group with the charge density distributed along both the HOMO and LUMO. We speculate that this shifts the band gap by effectively deprotonating the PEA and increasing the

https://doi.org/10.1021/acscentsci.2c00041
ACS Cent. Sci. 2022, 8, 571−580

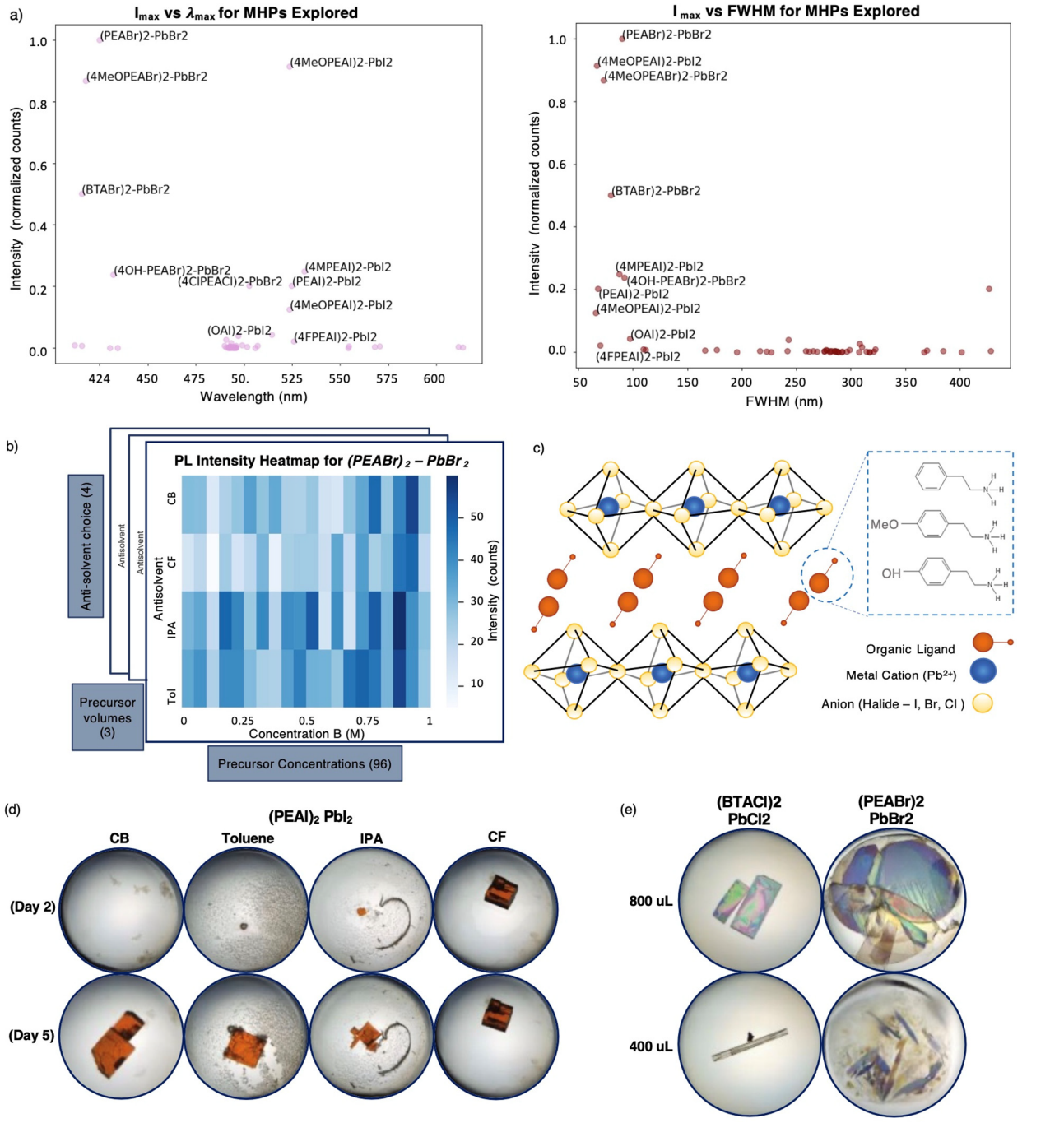

Figure 3. Analysis and visualizations of the experimental and chemical space explored in this work. (a) Data visualization of the chemical space explored in this work. (left) The brightest emission (I_{max}) for each material was normalized and plotted against the peak emission position (λ_{max}). (right) Full width at half-maximum (fwhm) for each material plotted against I_{max}. (b) Heat map visualization of the chemical space examined for each material. Each tray contains 288 different combinations of precursor concentration (96), solvent selection (2), antisolvent selection (4), and precursor volume (3). This plot displays the emission intensity of $(PEABr)_2$-$PbBr_2$ single crystals with increasing precursor concentration. (c) Schematic of a layered 2D MHP with a phenethylammonium organic spacer and a subset of the 54 organic spacer ligands explored in this work. (d) Temporal comparison of the crystallization process for the four antisolvents represented using $(PEAI)_2$-PbI_2. (e) Comparison between different precursor volumes for the same concentration and antisolvent combination.

electronegativity of the amino group.[57] Our observation is corroborated by a recent study in which 4-MeO-PEABr was used to tune the band edge and improve the charge balance and device performance of $CsPbBr_3$-based LEDs.[58] This result was also observed in the 4-MeO-PEAI perovskite that demonstrated a consistently narrower fwhm (~66 nm) and stronger emission during HTC than its nonfunctionalized parent ligand PEAI and OH-PEAI as seen in Figure 3a. Our results suggest that methoxy-functionalized PEA derivatives warrant further investigation by the broader research community.

The PEA derivatives shown in Figure 3c had an fwhm of <100 nm and a normalized PL ranging from 1 to 0.25, where 1 is the normalized I_{max} produced by our benchmark MHP,

https://doi.org/10.1021/acscentsci.2c00041
ACS Cent. Sci. 2022, 8, 571−580

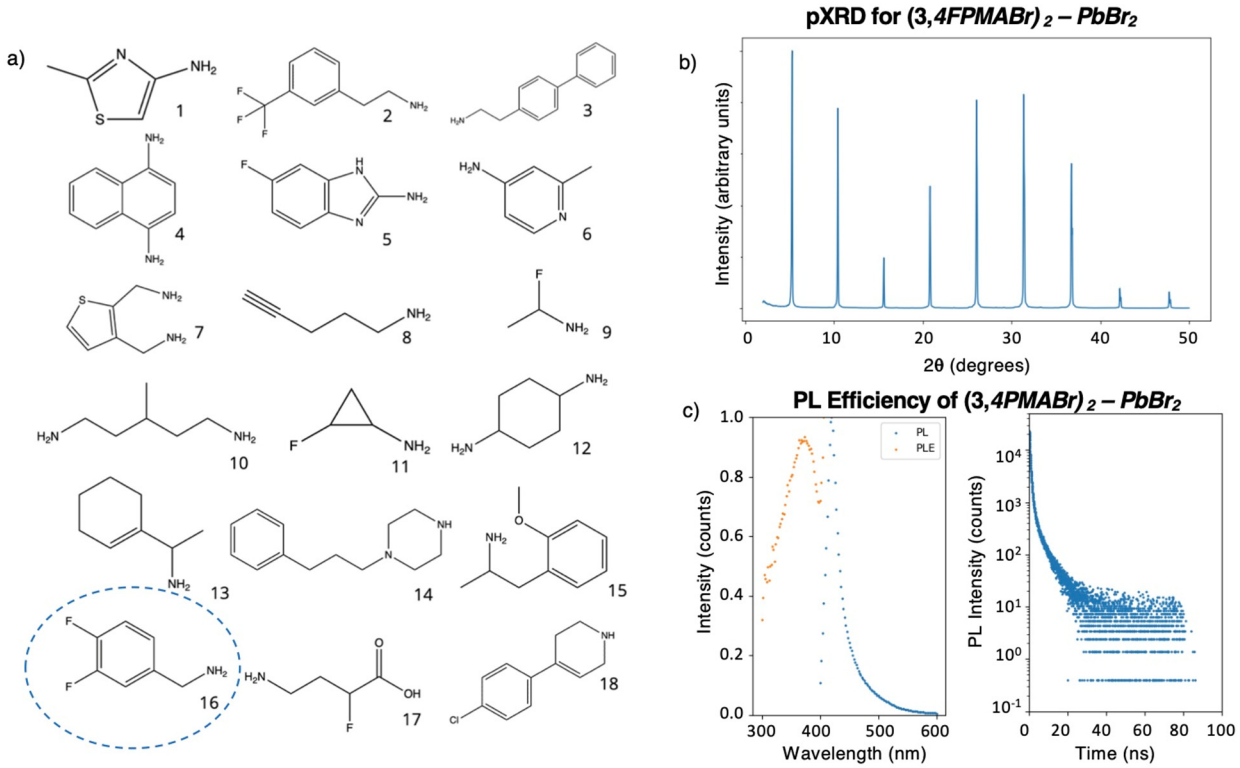

Figure 4. Molecules predicted and synthesized using our HTE screening process. (a) Eighteen organic spacers from the PubChem database screened based on Tanimoto similarity with the emitters discovered herein, and emitters found reported in the literature.[62] **1**, 2-Methylthiazol-4-amine; **2**, 2-(3-(trifluoromethyl)phenyl)ethanamine; **3**, 2-(4-biphenyl)ethylamine; **4**, 1,4-naphthalenediamine; **5**, 6-fluoro-1*H*-benzimidazol-2-amine; **6**, 4-amino-2-methylpyridine; **7**, thiophenebismethylamine; **8**, 4-pentyn-1-amine; **9**, 1-fluoroethanamine; **10**, 3-methylpentane-1,5-diamine; **11**, 2-fluorocyclopropanamine; **12**, cyclohexane-1,4-diamine; **13**, 1-(1-cyclohexenyl)ethylamine; **14**, 1-(3-phenylpropyl)piperazine; **15**, 2-methoxyamphetamine; **16**, 3,4-difluorophenylmethanamine; **17**, 4-amino-2-fluorobutanoic acid; **18**, 4-(4-chlorophenyl)-1,2,3,6-tetrahydropyridine. (b) Powder XRD of 3,4-difluorophenylmethanamine lead bromide ($(3,4\text{-FPMABr})_2\text{-PbBr}_2$), one of the 2D MHPs chosen from the PubChem database and synthesized for proof of concept yielding 10% PLQY. (c) PL, PLE, and PL lifetime for $(3,4\text{-FPMABr})_2\text{-PbBr}_2$.

$(PEABr)_2$-$PbBr_2$, which has been shown to have 80% PLQY.[53] 4-MeO-PEAI and 4-MeO-PEABr demonstrated normalized I_{max} values of 0.91 and 0.87, respectively. 4FPEAI was among the narrowest emitters (fwhm ∼ 69 nm), but its I_{max} was an order of magnitude lower than those of other PEAI compounds. 3FPEAI and FPEAI performed significantly worse with weak, broadband emission 3 orders of magnitude lower than those of the best emitters. A recent study on the systematic modification of diacetylphenylenediamines shows that compositionally engineering the A-site cation can lead to emission covering the entire visible color spectrum.[59] Similarly, our observations indicate a dependence between the functionalization of the phenyl group and both the color purity and PLQY of the emission.

Tanimoto Similarity for Potentially Bright MHPs. Unlike 3D perovskites, which can typically only incorporate a handful of cations at the A-site due to the geometric constraints of the interlayer space, 2D perovskites accept a wide variety of organic spacers. Our HTE exploration affords us multifaceted information that allows us to predict promising spacers for future experimental trials. The HTC methodology combined with unsupervised learning allowed us to quickly sift through a large chemical space and measure bright emitters. We fingerprinted these molecular structures and sifted through existing databases to identify potential similar candidates. To this end, we chose the Tanimoto index because it takes into account existing knowledge on the fingerprinted materials, as well as any bias. The Tanimoto index has been identified to be one of the best metrics for similarity calculations.[60]

To make our predictions, we clustered the data generated using the HTC and created a dissimilarity matrix that highlights differences in emission peaks (Figure S6).[61] This analysis gave insight into which ligands generate the brightest MHPs with the narrowest emission peaks. Molecules structurally similar to the brightest emitters in our data set, and materials previously reported in the literature,[62] were mined from the PubChem database (110 million compounds) using a Tanimoto score of 0.85 as the threshold. Of the identified molecules, only amines and ammonium halides were retained. Identified molecules were ranked using the criteria of charge (only +1, +2 allowed), degree of amine (1° > 2° > 3°), and ring size (diameter < width of MX_6 octahedron, 6.4 Å). The 18 most promising candidates are shown in Figure 4a.

The presented molecules can be identified as promising spacer candidates due to several characteristics. They feature one or two protonatable nitrogen molecules, resulting in perovskites with general formulas $A'_2A_{n-1}M_nX_{3n+1}$ and $A'A_{n-1}M_nX_3n_{+1}$, respectively. Higher charges are ruled out since they cannot achieve charge balance. The width of the molecules is smaller than the width of the MX_6 octahedron (6.4 Å). They do not contain bulky groups, which could sterically hinder the amino head from "locking" into the octahedron. Furthermore, the functional groups on the

https://doi.org/10.1021/acscentsci.2c00041
ACS Cent. Sci. 2022, 8, 571−580

molecules do not react with the solvents commonly used in synthesis: DMF, DMSO, and γ-butyrolactone (GBL).

For our proof of concept, we used one of the 18 predicted A-site ligands, 3,4-FPMA, to synthesize an MHP. The composition was upscaled into a macrocrystal and confirmed the layered structure of the MHP via powder X-ray diffraction (pXRD) (Figure 4b). The highly regular and low-angle diffraction peaks are characteristic of a 2D MHP.[63] We then exfoliated the macrocrystals and characterized their emission using an integrating sphere, obtaining a PLQY of 10%. The PL efficiency (PLE) and lifetime are shown in Figure 4c; this material will be optimized and studied further in future work.

CONCLUSIONS

We employed a high-throughput synthesis and characterization approach to study MHP single crystals using the VAAC synthesis method and demonstrated its effectiveness by optimizing the perovskite $(4\text{-MeO-PEAI})_2\text{-PbI}_2$. We then grew 16 128 MHP crystals and created the first known database of MHP light emission spectra. We analyzed the data generated to identify groups of materials that shared desired properties such as λ_{max}, I_{max}, color purity, and fwhm. We used this to identify the shared qualities of the brightest emitters and screened PubChem's database to generate 18 potential molecules based on Tanimoto similarity (Figure 3a). We synthesized one of the candidates (3,4-difluorobenzyl lead bromide) for proof of concept and achieved a PLQY of 10% on the exfoliated powder (Figure 3c). We present 17 additional candidates for future exploration, along with a rich database of over 100 000 crystal images, 16 128 PL spectra, and the corresponding synthesis parameters for future supervised machine learning. This work provides a benchmark for future efforts in the development of HTE methods for MHPs.

EXPERIMENTAL SECTION

General Experimental Procedures. Crystals were grown in high throughput by using VAAC synthesis described below. This synthesis process depends on precursor concentration as well as the choice of solvents and antisolvent. We initially experimented with eight antisolvents: methanol, dichlorobenzene, ethanol, butyl alcohol, toluene, IPA, CB, and CF. The first four antisolvents did not produce a high rate of crystallinity and were removed from our experimental parameters. We chose 12 ratios of DMF and DMSO per tray.

The crystals were imaged at regular intervals as they grew over the course of 7 days. Their emission was measured on the seventh day. Our HTC comprises two perpendicular motors, a 374 nm diode laser pulsed at a repetition rate of 100 MHz, and a detector (Ocean Optics 2000+ spectrometer) arranged in the configuration shown in Figure 1b.

We programmed two motors to sequentially move the Intelliplate bilaterally to each of the drops in the growth plate. A pulsed-laser excitation source is focused on each of the 288 drops via a mirror positioned 9 in. overhead. A detector attached to a collimated lens fitted with a UV filter is positioned at a 45° angle from the substrate and collects emission from the crystals in each drop. The laser excites the crystal within each drop, and the detector gathers the crystal's spectral PL response over a preprogrammed integration interval. We measure the emission from a tray comprised of drops filled with only solvent and subtract this blank from each measurement to account for any emission from the tray, solvent, and sealing tape. The resulting spectra have been compiled into a pandas dataframe[64] and uploaded to an online database along with the experimental parameters used to grow each crystal. The dataframe was augmented with the fwhm, λ_{max}, I_{max}, and theoretical calculations of the HOMO−LUMO band gap, formation energy, and density of states. This data was clustered, visualized, and analyzed to identify groups of materials that share desired properties such as I_{max}, λ_{max}, and narrow fwhm (Figure 3a). The brightest emitters were identified, and structurally similar molecules were mined from the PubChem database by using the Tanimoto similarity described below.

High-Throughput Synthesis. Precursor solutions were prepared by dissolving a lead halide ($PbBr_2$, $PbCl_2$, or PbI_2) and an organic salt (e.g., PEABr, 4-MeO-PEABr) in DMF or DMSO or both. The initial concentration was kept as high as possible without initiating precipitation, ranging from 2 to 0.25 M. Precursor and solvent solutions were added to the droplet wells of chemically resistant crystallization plates (three-well Intelliplates, Art Robbins Instruments, Figure 1a) with a Formulatrix NT8 fluid dispenser (Figure 1b). Antisolvents were added manually to the reservoirs of the synthesis plates with the use of a 12-channel pipettor. The Formulatrix NT8 drop setter was controlled with an XML code generated with a home-built python script that combinatorically combined solvent and precursors into the drops as programmed.

Macrocrystal Synthesis. The optimal precursor concentration and antisolvent choice was determined by analyzing the results of the HTE. The precursor solution was prepared at the desired concentration, and 1 mL was placed into a vial which was placed in a larger vial with 3 mL of antisolvent. To form single macrocrystals, the vials were placed in an airtight container lined with a desiccant for humidity control and left in a fume hood undisturbed for approximately 6−10 days.

Data Analysis. The Tanimoto coefficient is used as a measure of structural similarity.[60] A coefficient of 0 indicates no similarity, and 1 may indicate identity between two molecules. The coefficient is calculated as a function of binary fingerprints of the two structures. The fingerprint is a binary number with each bit encoding the presence or absence of predefined structure fragments or a feature in the structure such as rings, nearest neighbors, and elements. Here, the PubChem fingerprint is used, which encodes information with 881 binary digits, using seven groups of hierarchical features.[65] The Tanimoto coefficient is calculated as

$$T = \frac{N_{A\&B}}{N_A + N_B - N_{A\&B}}$$

where N_A represents the number of "on" bits in structure A, N_B represents the number of "on" bits in structure B, and $N_{A\&B}$ represents the number of "on" bits common to both. The PubChem PUG REST API was used to sift through the PubChem database for molecules that match the query with a Tanimoto coefficient of >0.85. The threshold of 0.85 is borrowed from computational drug discovery, where a Tanimoto coefficient of 0.85 is widely used as an indicator that the two compounds share similar activities.[66]

Density Functional Theory Calculations. PEABr, OH-PEABr, and MeO-PEABr structures were optimized under the PBE/DZVP-MOLOPT-SR-GTH level of theory with GTH-PBE pseudopotentials using the CP2K package (version 6.1).[67,67−69] The ligands were optimized individually, before

https://doi.org/10.1021/acscentsci.2c00041
ACS Cent. Sci. 2022, 8, 571−580

attachment to PbBr cores representing the perovskite crystal, and the resulting electron density and electronic properties were extracted. Excitation energies and HOMO−LUMO band gap were then used to supplement the spectra observed.

Powder XRD Measurements. The crystals were upscaled to >1 mm^3, rinsed with IPA, and crushed into a powder. X-ray diffraction measurements were conducted with a Rigaku MiniFlex 6G 600 instrument (Bragg−Brentano geometry) equipped with a D/teX Ultra silicon strip detector and a Cu Kα radiation source (λ = 1.5406 Å) operating at a voltage of 40 kV and a current of 15 mA.

Optical Measurements. The crystals were upscaled to >1 mm^3, rinsed with IPA, and crushed into a powder, and sealed between two glass slides. Absorption was measured with a PerkinElmer 950 UV/vis/NIR spectrometer equipped with an integrating sphere for thin-film measurements. PL quantum yield and PL decay measurements were carried out with a Horiba FluoroLog-3 spectrofluorometer in reflection geometry under ambient conditions. The sample was excited with monochromated light (375 nm) from a xenon lamp. The emission was passed through a 500 nm blaze grating monochromator (iHR320) and collected by an infrared photomultiplier tube.

■ ASSOCIATED CONTENT

Supporting Information

The Supporting Information is available free of charge at https://pubs.acs.org/doi/10.1021/acscentsci.2c00041.

DFT results; materials explored; additional data analysis (PDF)

HTE Fabrication: The Formulatrix NT8 drop setter combinatorically combines solvent and precursors into the drops as programmed (MP4)

HTE Imaging: An automated imaging system scans each tray and captures multiple images of each drop at pre-programmed intervals (MP4)

HTE Characterization: Two motors sequentially move the growth plate bilaterally to each of the drops. A pulsed laser excites the crystals and a detector gathers the crystal's emission from each drop (MP4)

■ AUTHOR INFORMATION

Corresponding Author

Edward H. Sargent − *The Edward S. Rogers Department of Electrical and Computer Engineering, University of Toronto, Toronto, Ontario, Canada M5S 3G4;* orcid.org/0000-0003-0396-6495; Email: ted.sargent@utoronto.ca

Authors

Husna Anwar − *The Edward S. Rogers Department of Electrical and Computer Engineering, University of Toronto, Toronto, Ontario, Canada M5S 3G4*

Andrew Johnston − *The Edward S. Rogers Department of Electrical and Computer Engineering, University of Toronto, Toronto, Ontario, Canada M5S 3G4;* orcid.org/0000-0002-4545-532X

Suhas Mahesh − *The Edward S. Rogers Department of Electrical and Computer Engineering, University of Toronto, Toronto, Ontario, Canada M5S 3G4*

Kamalpreet Singh − *Department of Physical and Environmental Sciences, University of Toronto Scarborough, Scarborough, Ontario, Canada M1C 1A4;* orcid.org/0000-0001-8569-1119

Zhibo Wang − *Department of Physical and Environmental Sciences, University of Toronto Scarborough, Scarborough, Ontario, Canada M1C 1A4*

Douglas A. Kuntz − *Princess Margaret Cancer Centre, University Health Network, Toronto, Ontario, Canada M5G 1L7*

Isaac Tamblyn − *Department of Physics, University of Ottawa, Vector Institute for Artificial Intelligence, Ottawa, Ontario, Canada K1N 6N5;* orcid.org/0000-0002-8146-6667

Oleksandr Voznyy − *Department of Physical and Environmental Sciences, University of Toronto Scarborough, Scarborough, Ontario, Canada M1C 1A4;* orcid.org/0000-0002-8656-5074

Gilbert G. Privé − *Princess Margaret Cancer Centre, University Health Network, Toronto, Ontario, Canada M5G 1L7; Department of Medical Biophysics, University of Toronto, Toronto, Ontario, Canada M5G 1L7; Department of Biochemistry, University of Toronto, Toronto, Ontario, Canada M5S 1A8;* orcid.org/0000-0002-0712-4319

Complete contact information is available at: https://pubs.acs.org/10.1021/acscentsci.2c00041

Author Contributions

$^{\nabla}$H.A. and A.J. contributed equally.

Funding

This work was supported by the Alliance for AI-Accelerated Materials Discovery (A3MD), whose funding members for this work included LG and TotalEnergies. It was also funded by the Natural Sciences and Engineering Research Council (NSERC) of Canada. Computations were performed on the Niagara supercomputer at the SciNet HPC Consortium. SciNet is funded by the Canada Foundation for Innovation, the Government of Ontario, Ontario Research Fund—Research Excellence, and the University of Toronto.

Notes

The authors declare no competing financial interest.

Some Python scripts used for data analysis and a sample data set can be found in the GitHub repository at https://github.com/husnaanwar/mhp_light_emission. Please contact authors for full data set.

■ ACKNOWLEDGMENTS

The authors thank L. Levina, E. Palmiano, R. Wolowiec, D. Kopilovic, and J. Karlen for their assistance during the period of study.

■ REFERENCES

(1) Sutherland, B. R.; Sargent, E. H. Perovskite Photonic Sources. *Nat. Photonics* **2016**, *10* (5), 295−302.

(2) Hoye, R. L. Z.; Fakharuddin, A.; Congreve, D. N.; Wang, J.; Schmidt-Mende, L. Light Emission from Perovskite Materials. *APL Mater.* **2020**, *8* (7), 070401.

(3) Stranks, S. D.; Eperon, G. E.; Grancini, G.; Menelaou, C.; Alcocer, M. J. P.; Leijtens, T.; Herz, L. M.; Petrozza, A.; Snaith, H. J. Electron-Hole Diffusion Lengths Exceeding 1 Micrometer in an Organometal Trihalide Perovskite Absorber. *Science* **2013**, *342* (6156), 341−344.

(4) Stranks, S. D.; Burlakov, V. M.; Leijtens, T.; Ball, J. M.; Goriely, A.; Snaith, H. J. Recombination Kinetics in Organic-Inorganic Perovskites: Excitons, Free Charge, and Subgap States. *Phys. Rev. Appl.* **2014**, *2* (3), 034007.

(5) Shi, D.; Adinolfi, V.; Comin, R.; Yuan, M.; Alarousu, E.; Buin, A.; Chen, Y.; Hoogland, S.; Rothenberger, A.; Katsiev.; et al. Low Trap-State Density and Long Carrier Diffusion in Organolead Trihalide Perovskite Single Crystals. *Science* **2015**, *347* (6221), 519−522.
(6) Xing, G.; Mathews, N.; Sun, S.; Lim, S. S.; Lam, Y. M.; Grätzel, M.; Mhaisalkar, S.; Sum, T. C. Long-Range Balanced Electron-and Hole-Transport Lengths in Organic-Inorganic CH3NH3PbI3. *Science* **2013**, *342* (6156), 344−347.
(7) Dolzhenko, Y. I.; Inabe, T.; Maruyama, Y. In Situ X-Ray Observation on the Intercalation of Weak Interaction Molecules into Perovskite-Type Layered Crystals (C9H19NH3)2PbI4 and (C10H21NH3)2CdCl4. *Bull. Chem. Soc. Jpn.* **1986**, *59* (2), 563−567.
(8) Dou, L. Emerging Two-Dimensional Halide Perovskite Nanomaterials. *J. Mater. Chem. C* **2017**, *5* (43), 11165−11173.
(9) Chen, S.; Shi, G. Two-Dimensional Materials for Halide Perovskite-Based Optoelectronic Devices. *Adv. Mater.* **2017**, *29* (24), 1605448.
(10) Kim, E.-B.; Akhtar, M. S.; Shin, H.-S.; Ameen, S.; Nazeeruddin, M. K. A Review on Two-Dimensional (2D) and 2D-3D Multidimensional Perovskite Solar Cells: Perovskites Structures, Stability, and Photovoltaic Performances. *J. Photochem. Photobiol. C Photochem. Rev.* **2021**, *48*, 100405.
(11) Stoumpos, C.; Cao, D.; Clark, D.; Young, J.; Rondinelli, J.; Jang, J.; Hupp, J.; Kanatzidis, M. Ruddlesden-Popper Hybrid Lead Iodide Perovskite 2D Homologous Semiconductors. *Chem. Mater.* **2016**, *28*, 2852−2867.
(12) Yuan, M.; Quan, L. N.; Comin, R.; Walters, G.; Sabatini, R.; Voznyy, O.; Hoogland, S.; Zhao, Y.; Beauregard, E. M.; Kanjanaboos, P.; et al. Perovskite Energy Funnels for Efficient Light-Emitting Diodes. *Nat. Nanotechnol.* **2016**, *11* (10), 872−877.
(13) Byun, J.; Cho, H.; Wolf, C.; Jang, M.; Sadhanala, A.; Friend, R. H.; Yang, H.; Lee, T.-W. Efficient Visible Quasi-2D Perovskite Light-Emitting Diodes. *Adv. Mater.* **2016**, *28* (34), 7515−7520.
(14) Quan, L. N.; García de Arquer, F. P.; Sabatini, R. P.; Sargent, E. H. Perovskites for Light Emission. *Adv. Mater.* **2018**, *30* (45), 1801996.
(15) Mitzi, D. B.; Feild, C. A.; Harrison, W. T. A.; Guloy, A. M. Conducting Tin Halides with a Layered Organic-Based Perovskite Structure. *Nature* **1994**, *369* (6480), 467−469.
(16) Hua, Y.; Zhou, Y.; Hong, D.; Wan, S.; Hu, X.; Xie, D.; Tian, Y. Identification of the Band Gap Energy of Two-Dimensional (OA)2(MA)N−1PbnI3n+1 Perovskite with up to 10 Layers. *J. Phys. Chem. Lett.* **2019**, *10* (22), 7025−7030.
(17) Even, J.; Pedesseau, L.; Katan, C. Understanding Quantum Confinement of Charge Carriers in Layered 2D Hybrid Perovskites. *ChemPhysChem* **2014**, *15* (17), 3733−3741.
(18) Miyata, A.; Mitioglu, A.; Plochocka, P.; Portugall, O.; Wang, J. T.-W.; Stranks, S. D.; Snaith, H. J.; Nicholas, R. J. Direct Measurement of the Exciton Binding Energy and Effective Masses for Charge Carriers in Organic−Inorganic Tri-Halide Perovskites. *Nat. Phys.* **2015**, *11* (7), 582−587.
(19) Yang, Y.; Ostrowski, D. P.; France, R. M.; Zhu, K.; van de Lagemaat, J.; Luther, J. M.; Beard, M. C. Observation of a Hot-Phonon Bottleneck in Lead-Iodide Perovskites. *Nat. Photonics* **2016**, *10* (1), 53−59.
(20) García-Benito, I.; Quarti, C.; Queloz, V. I. E.; Hofstetter, Y. J.; Becker-Koch, D.; Caprioglio, P.; Neher, D.; Orlandi, S.; Cavazzini, M.; Pozzi, G.; Even, J.; et al. Fluorination of Organic Spacer Impacts on the Structural and Optical Response of 2D Perovskites. *Front. Chem.* **2020**, *7*, 946.
(21) Mao, L.; Wu, Y.; Stoumpos, C. C.; Traore, B.; Katan, C.; Even, J.; Wasielewski, M. R.; Kanatzidis, M. G. Tunable White-Light Emission in Single-Cation-Templated Three-Layered 2D Perovskites (CH3CH2NH3)4Pb3Br10−XClx. *J. Am. Chem. Soc.* **2017**, *139* (34), 11956−11963.
(22) Senanayak, S. P.; Yang, B.; Thomas, T. H.; Giesbrecht, N.; Huang, W.; Gann, E.; Nair, B.; Goedel, K.; Guha, S.; Moya, X.; McNeill, C. R.; et al. Understanding Charge Transport in Lead Iodide Perovskite Thin-Film Field-Effect Transistors. *Sci. Adv.* **2017**, *3* (1), e1601935.
(23) Zhang, F.; Zhang, H.; Zhu, L.; Qin, L.; Wang, Y.; Hu, Y.; Lou, Z.; Hou, Y.; Teng, F. Two-Dimensional Organic−Inorganic Hybrid Perovskite Field-Effect Transistors with Polymers as Bottom-Gate Dielectrics. *J. Mater. Chem. C* **2019**, *7* (14), 4004−4012.
(24) Chen, Y.; Sun, Y.; Peng, J.; Tang, J.; Zheng, K.; Liang, Z. 2D Ruddlesden−Popper Perovskites for Optoelectronics. *Adv. Mater.* **2018**, *30* (2), 1703487.
(25) Blancon, J.-C.; Tsai, H.; Nie, W.; Stoumpos, C. C.; Pedesseau, L.; Katan, C.; Kepenekian, M.; Soe, C. M. M.; Appavoo, K.; Sfeir, M. Y.; et al. Extremely Efficient Internal Exciton Dissociation through Edge States in Layered 2D Perovskites. *Science* **2017**, *355* (6331), 1288−1292.
(26) Lin, K.; Xing, J.; Quan, L. N.; de Arquer, F. P. G.; Gong, X.; Lu, J.; Xie, L.; Zhao, W.; Zhang, D.; Yan, C.; et al. Perovskite Light-Emitting Diodes with External Quantum Efficiency Exceeding 20 per Cent. *Nature* **2018**, *562* (7726), 245−248.
(27) Yuan, F.; Zheng, X.; Johnston, A.; Wang, Y.-K.; Zhou, C.; Dong, Y.; Chen, B.; Chen, H.; Fan, J. Z.; Sharma, G.; et al. Color-Pure Red Light-Emitting Diodes Based on Two-Dimensional Lead-Free Perovskites. *Sci. Adv.* **2020**, *6* (42), eabb0253.
(28) Zhang, L.; Sun, C.; He, T.; Jiang, Y.; Wei, J.; Huang, Y.; Yuan, M. High-Performance Quasi-2D Perovskite Light-Emitting Diodes: From Materials to Devices. *Light Sci. Appl.* **2021**, *10* (1), 61.
(29) Gangishetty, M. K.; Hou, S.; Quan, Q.; Congreve, D. N. Reducing Architecture Limitations for Efficient Blue Perovskite Light-Emitting Diodes. *Adv. Mater.* **2018**, *30* (20), 1706226.
(30) Unger, E. L.; Bowring, A. R.; Tassone, C. J.; Pool, V. L.; Gold-Parker, A.; Cheacharoen, R.; Stone, K. H.; Hoke, E. T.; Toney, M. F.; McGehee, M. D. Chloride in Lead Chloride-Derived Organo-Metal Halides for Perovskite-Absorber Solar Cells. *Chem. Mater.* **2014**, *26* (24), 7158−7165.
(31) Ren, Z.; Wang, K.; Sun, X. W.; Choy, W. C. H. Strategies Toward Efficient Blue Perovskite Light-Emitting Diodes. *Adv. Funct. Mater.* **2021**, *31* (30), 2100516.
(32) Kumawat, N. K.; Liu, X.-K.; Kabra, D.; Gao, F. Blue Perovskite Light-Emitting Diodes: Progress, Challenges and Future Directions. *Nanoscale* **2019**, *11* (5), 2109−2120.
(33) Ge, C.; Fang, Q.; Lin, H.; Hu, H. Review on Blue Perovskite Light-Emitting Diodes: Recent Advances and Future Prospects. *Front. Mater.* **2021**, *8*, 15.
(34) Li, X.; Hoffman, J. M.; Kanatzidis, M. G. The 2D Halide Perovskite Rulebook: How the Spacer Influences Everything from the Structure to Optoelectronic Device Efficiency. *Chem. Rev.* **2021**, *121* (4), 2230−2291.
(35) Kumar, S.; Jagielski, J.; Yakunin, S.; Rice, P.; Chiu, Y.-C.; Wang, M.; Nedelcu, G.; Kim, Y.; Lin, S.; et al. Efficient Blue Electroluminescence Using Quantum-Confined Two-Dimensional Perovskites. *ACS Nano* **2016**, *10* (10), 9720−9729.
(36) Xing, J.; Zhao, Y.; Askerka, M.; Quan, L. N.; Gong, X.; Zhao, W.; Zhao, J.; Tan, H.; Long, G.; Gao, L.; et al. Color-Stable Highly Luminescent Sky-Blue Perovskite Light-Emitting Diodes. *Nat. Commun.* **2018**, *9* (1), 3541.
(37) Sadhanala, A.; Ahmad, S.; Zhao, B.; Giesbrecht, N.; Pearce, P. M.; Deschler, F.; Hoye, R. L. Z.; Gödel, K. C.; Bein, T.; et al. Blue-Green Color Tunable Solution Processable Organolead Chloride−Bromide Mixed Halide Perovskites for Optoelectronic Applications. *Nano Lett.* **2015**, *15* (9), 6095−6101.
(38) Maier, W. F. Early Years of High-Throughput Experimentation and Combinatorial Approaches in Catalysis and Materials Science. *ACS Comb. Sci.* **2019**, *21* (6), 437−444.
(39) Ludwig, A. Discovery of New Materials Using Combinatorial Synthesis and High-Throughput Characterization of Thin-Film Materials Libraries Combined with Computational Methods. *Npj Comput. Mater.* **2019**, *5* (1), 1−7.
(40) Stroyuk, O.; Raievska, O.; Langner, S.; Kupfer, C.; Barabash, A.; Solonenko, D.; Azhniuk, Y.; Hauch, J.; Osvet, A.; et al. High-Throughput Robotic Synthesis and Photoluminescence Character-

https://doi.org/10.1021/acscentsci.2c00041
ACS Cent. Sci. 2022, 8, 571−580

ization of Aqueous Multinary Copper−Silver Indium Chalcogenide Quantum Dots. *Part. Part. Syst. Charact.* **2021**, *38*, 2100169.
(41) Du, J. S.; Shin, D.; Stanev, T. K.; Musumeci, C.; Xie, Z.; Huang, Z.; Lai, M.; Sun, L.; Zhou, W.; Stern, N. P.; et al. Halide Perovskite Nanocrystal Arrays: Multiplexed Synthesis and Size-Dependent Emission. *Sci. Adv.* **2020**, *6* (39), eabc4959.
(42) Li, S.; Baker, R. W.; Lignos, I.; Yang, Z.; Stavrakis, S.; Howes, P. D.; deMello, A. J. Automated Microfluidic Screening of Ligand Interactions during the Synthesis of Cesium Lead Bromide Nanocrystals. *Mol. Syst. Des. Eng.* **2020**, *5* (6), 1118−1130.
(43) Reinhardt, E.; Salaheldin, A. M.; Distaso, M.; Segets, D.; Peukert, W. Rapid Characterization and Parameter Space Exploration of Perovskites Using an Automated Routine. *ACS Comb. Sci.* **2020**, *22* (1), 6−17.
(44) Chen, S.; Hou, Y.; Chen, H.; Tang, X.; Langner, S.; Li, N.; Stubhan, T.; Levchuk, I.; Gu, E.; et al. Exploring the Stability of Novel Wide Bandgap Perovskites by a Robot Based High Throughput Approach. *Adv. Energy Mater.* **2018**, *8* (6), 1701543.
(45) Sun, S.; Hartono, N. T. P.; Ren, Z. D.; Oviedo, F.; Buscemi, A. M.; Layurova, M.; Chen, D. X.; Ogunfunmi, T.; Thapa, J.; Ramasamy, S.; et al. Accelerated Development of Perovskite-Inspired Materials via High-Throughput Synthesis and Machine-Learning Diagnosis. *Joule* **2019**, *3* (6), 1437−1451.
(46) Saidaminov, M. I.; Adinolfi, V.; Comin, R.; Abdelhady, A. L.; Peng, W.; Dursun, I.; Yuan, M.; Hoogland, S.; Sargent, E. H.; Bakr, O. M. Planar-Integrated Single-Crystalline Perovskite Photodetectors. *Nat. Commun.* **2015**, *6* (1), 8724.
(47) Konstantakou, M.; Perganti, D.; Falaras, P.; Stergiopoulos, T. Anti-Solvent Crystallization Strategies for Highly Efficient Perovskite Solar Cells. *Crystals* **2017**, *7* (10), 291.
(48) Müller, P. Practical Suggestions for Better Crystal Structures. *Crystallogr. Rev.* **2009**, *15* (1), 57−83.
(49) Chen, Q.; Zhou, H.; Hong, Z.; Luo, S.; Duan, H.-S.; Wang, H.-H.; Liu, Y.; Li, G.; Yang, Y. Planar Heterojunction Perovskite Solar Cells via Vapor-Assisted Solution Process. *J. Am. Chem. Soc.* **2014**, *136* (2), 622−625.
(50) Karlsson, M.; Yi, Z.; Reichert, S.; Luo, X.; Lin, W.; Zhang, Z.; Bao, C.; Zhang, R.; Bai, S.; Zheng, G.; et al. Mixed Halide Perovskites for Spectrally Stable and High-Efficiency Blue Light-Emitting Diodes. *Nat. Commun.* **2021**, *12* (1), 361.
(51) Kirman, J.; Johnston, A.; Kuntz, D. A.; Askerka, M.; Gao, Y.; Todorović, P.; Ma, D.; Privé, G. G.; Sargent, E. H. Machine-Learning-Accelerated Perovskite Crystallization. *Matter* **2020**, *2* (4), 938−947.
(52) *NT8 - Drop Setter*. Formulatrix. https://formulatrix.com/protein-crystallization-systems/nt8-drop-setter/ (accessed 2021-09-13).
(53) Gong, X.; Voznyy, O.; Jain, A.; Liu, W.; Sabatini, R.; Piontkowski, Z.; Walters, G.; Bappi, G.; Nokhrin, S.; et al. Electron−Phonon Interaction in Efficient Perovskite Blue Emitters. *Nat. Mater.* **2018**, *17* (6), 550−556.
(54) Jeon, N. J.; Noh, J. H.; Kim, Y. C.; Yang, W. S.; Ryu, S.; Seok, S. I. Solvent Engineering for High-Performance Inorganic−Organic Hybrid Perovskite Solar Cells. *Nat. Mater.* **2014**, *13* (9), 897−903.
(55) Tidhar, Y.; Edri, E.; Weissman, H.; Zohar, D.; Hodes, G.; Cahen, D.; Rybtchinski, B.; Kirmayer, S. Crystallization of Methyl Ammonium Lead Halide Perovskites: Implications for Photovoltaic Applications. *J. Am. Chem. Soc.* **2014**, *136* (38), 13249−13256.
(56) Cacciuto, A.; Auer, S.; Frenkel, D. Onset of Heterogeneous Crystal Nucleation in Colloidal Suspensions. *Nature* **2004**, *428* (6981), 404−406.
(57) Colthup, N. B.; Daly, L. H.; Wiberley, S. E. Ethers, Alcohols, and Phenols. In *Introduction to Infrared and Raman Spectroscopy*; Elsevier: 1990; pp 327−337. DOI: 10.1016/B978-0-08-091740-5.50013-2.
(58) Worku, M.; Ben-Akacha, A.; Sridhar, S.; Frick, J. R.; Yin, S.; He, Q.; Robb, A. J.; Chaaban, M.; Liu, H.; et al. Band Edge Control of Quasi-2D Metal Halide Perovskites for Blue Light-Emitting Diodes with Enhanced Performance. *Adv. Funct. Mater.* **2021**, *31*, 2103299.
(59) Kim, H.; Park, W.; Kim, Y.; Filatov, M.; Choi, C. H.; Lee, D. Relief of Excited-State Antiaromaticity Enables the Smallest Red Emitter. *Nat. Commun.* **2021**, *12* (1), 5409.
(60) Bajusz, D.; Rácz, A.; Héberger, K. Why Is Tanimoto Index an Appropriate Choice for Fingerprint-Based Similarity Calculations. *J. Cheminformatics* **2015**, *7* (1), 20.
(61) Pedregosa, F.; Varoquaux, G.; Gramfort, A.; Michel, V.; Thirion, B.; Grisel, O.; Blondel, M.; Prettenhofer, P.; Weiss, R.; et al. Scikit-Learn: Machine Learning in Python. *J. Mach. Learn. Res.* **2011**, *12* (85), 2825−2830.
(62) Mao, L.; Stoumpos, C. C.; Kanatzidis, M. G. Two-Dimensional Hybrid Halide Perovskites: Principles and Promises. *J. Am. Chem. Soc.* **2019**, *141* (3), 1171−1190.
(63) Quintero-Bermudez, R.; Gold-Parker, A.; Proppe, A. H.; Munir, R.; Yang, Z.; Kelley, S. O.; Amassian, A.; Toney, M. F.; Sargent, E. H. Compositional and Orientational Control in Metal Halide Perovskites of Reduced Dimensionality. *Nat. Mater.* **2018**, *17* (10), 900−907.
(64) Anwar, H. *High-Throughput Evaluation of Emission and Structure in Perovskite Light Emission*. 2021. https://github.com/husnaanwar/mhp_light_emission.
(65) *PubChem Substructure Fingerprint*. https://pubchem.ncbi.nlm.nih.gov/.
(66) Patterson, D. E.; Cramer, R. D.; Ferguson, A. M.; Clark, R. D.; Weinberger, L. E. Neighborhood Behavior: A Useful Concept for Validation of "Molecular Diversity" Descriptors. *J. Med. Chem.* **1996**, *39* (16), 3049−3059.
(67) Grimme, S.; Antony, J.; Ehrlich, S.; Krieg, H. A Consistent and Accurate Ab Initio Parametrization of Density Functional Dispersion Correction (DFT-D) for the 94 Elements H-Pu. *J. Chem. Phys.* **2010**, *132* (15), 154104.
(68) Kirklin, S.; Saal, J. E.; Meredig, B.; Thompson, A.; Doak, J. W.; Aykol, M.; Rühl, S.; Wolverton, C. The Open Quantum Materials Database (OQMD): Assessing the Accuracy of DFT Formation Energies. *npj Comput. Mater.* **2015**, *1* (1), 15010.
(69) Hutter, J.; Iannuzzi, M.; Schiffmann, F.; VandeVondele, J. Cp2k: Atomistic Simulations of Condensed Matter Systems. *WIREs Comput. Mol. Sci.* **2014**, *4* (1), 15−25.

https://doi.org/10.1021/acscentsci.2c00041
ACS Cent. Sci. 2022, 8, 571−580